sustainability

MDPI

Article

Can Drones Map Earth Cracks? Landslide Measurements in North Greece Using UAV Photogrammetry for Nature-Based Solutions

Paschalis D. Koutalakis [1], Ourania A. Tzoraki [1], Georgios I. Prazioutis [2], Georgios T. Gkiatas [3] and George N. Zaimes [3,*]

[1] Department of Marine Sciences, University of the Aegean, University Hill, 81100 Mytilene, Greece; koutalakis_p@yahoo.gr (P.D.K.); rania.tzoraki@aegean.gr (O.A.T.)
[2] Department of Surveying and Geoinformatics Engineering, International Hellenic University, University Campus Magnisias, 62124 Serres, Greece; giorgospraz@gmail.com
[3] UNESCO Chair Con-E-Ect, Department of Forest and Natural Environment Sciences, International Hellenic University, University Campus Drama, 1st km Drama-Mikrohoriou, 66100 Drama, Greece; george.giatas@hotmail.com
* Correspondence: zaimesg@for.ihu.gr; Tel.: +30-2521-060-411

Abstract: The accuracy of photogrammetry for geohazards monitoring has improved within the last years because of the "drone revolution". This study is an attempt to perform morphometric measurements in a landslide event that took place near the village Nea Zichni in Northern Greece. The DJI Mavic 2 Pro was selected to capture orthoimages of the entire area including the landslide event but also other adjusted disaster phenomena. The images were loaded in the commercial software Pix4D in order to produce orthomosaics and digital surface models of the area. The georeferenced results were further analyzed in ArcGIS in order to digitize and estimate the morphometric parameters of the landslide, such as its area and volume, but also to detect cracks and plot the tensile cracking directions. We conclude that the methodology and produced outputs are crucial for the responsible authorities to detect, monitor and mitigate natural disasters such as landslide events and other mass movements. The best practices to control mass movements are nature-based solutions such as soil bioengineering and proper vegetation cover assisted by engineering measures. Finally, our goal is to frequently monitor the landslide phenomenon in order to determine its evolution.

Keywords: drone; DSM; fissures; geohazard; GIS; mapping; natural disaster; nature-based solutions; orthomosaic; UAS

check for updates

Citation: Koutalakis, P.D.; Tzoraki, O.A.; Prazioutis, G.I.; Gkiatas, G.T.; Zaimes, G.N. Can Drones Map Earth Cracks? Landslide Measurements in North Greece Using UAV Photogrammetry for Nature-Based Solutions. *Sustainability* **2021**, *13*, 4697. https://doi.org/10.3390/su13094697

Academic Editor: Alejandro Gonzalez-Ollauri

Received: 15 March 2021
Accepted: 19 April 2021
Published: 22 April 2021

Publisher's Note: MDPI stays neutral with regard to jurisdictional claims in published maps and institutional affiliations.

Copyright: © 2021 by the authors. Licensee MDPI, Basel, Switzerland. This article is an open access article distributed under the terms and conditions of the Creative Commons Attribution (CC BY) license (https://creativecommons.org/licenses/by/4.0/).

1. Introduction

The definition of the landslide hazard is difficult because it is a very complex natural (or even man-triggered) phenomenon [1]. A landslide is "a process of changes in the stress–strain state of a slope groundmass leading to a mass separation and ground movement downslope, while maintaining a continuous contact between sliding mass and underlying undisturbed ground" [2]. This specific definition of "landslide" excludes other related types of slope failures such as subsidence, toppling and rockfall [3,4]. In general, a landslide develops in time through several stages (prefailure deformations, failure itself and postfailure displacements) but it can also be a sudden event. Additionally, there are landslides with many movement episodes, separated by long or short periods of relative inactivity [5]. Landslides are complicated phenomena and may exhibit many different slope failures apart from the main soil slump, e.g., topples, rockfall, subsidence, creep, etc. while typical and profound types of fractures are the tensile cracks or fissures (Figure 1) [6,7].

Geohazards such as landslides, mass movements, subsidence and sinkholes have been recorded in many areas of Greece (Florina, Thessaloniki, Thessaly, etc.) [8–10] as well as in other parts of the world (Ebro River in Spain, Mexico City, Venice in Italy, etc.) [11–13]. Most

of these cases are characterized by the presence of loose sedimentary deposits with confined or semiconfined aquifers, as well as artesian aquifers [14,15]. Slope saturation by water is a primary cause of landslides. This can occur by extreme precipitation events [16], by active faults and earthquakes [17], by intense human activities, constructions and urbanization causes [18,19], by climate change in permafrost regions [20] and by sea level rise in coastal areas (including tsunamis) [21,22].

Landslides and other catastrophic events have significant impacts on human communities and can result in several kinds of damage, such as economic losses and, in the worst cases, casualties [23,24]. Monitoring is mandatory in order to investigate such phenomena, to assess the possible triggering factors and to measure the evolution of the postemergency phase. There are various methods, tools and approaches for landslide monitoring that include geophones and inclinometers, topographical survey measurements with total stations or Global Navigation Satellite Systems (GNSS) receivers, Airborne Light Detection and Ranging (LiDAR) systems, Terrestrial Laser Scanners (TLSs), photogrammetric techniques using aerial photos or high resolution satellite images, Differential Interferometry using radar images (DInSAR) and photogrammetric techniques using data from Unmanned Aerial Vehicles (UAVs) [25–28]. A successful innovative example is the LITMUS landslide detection system, which provides a web portal and a live demonstration map of the events. The LITMUS combines multiple physical sensors such as near real-time data from the United States Geological Survey (USGS) seismic network, the Tropical Rainfall Measuring Mission by National Aeronautics and Space Administration (NASA), but also reports from social media, e.g., Twitter, YouTube, and Instagram [29].

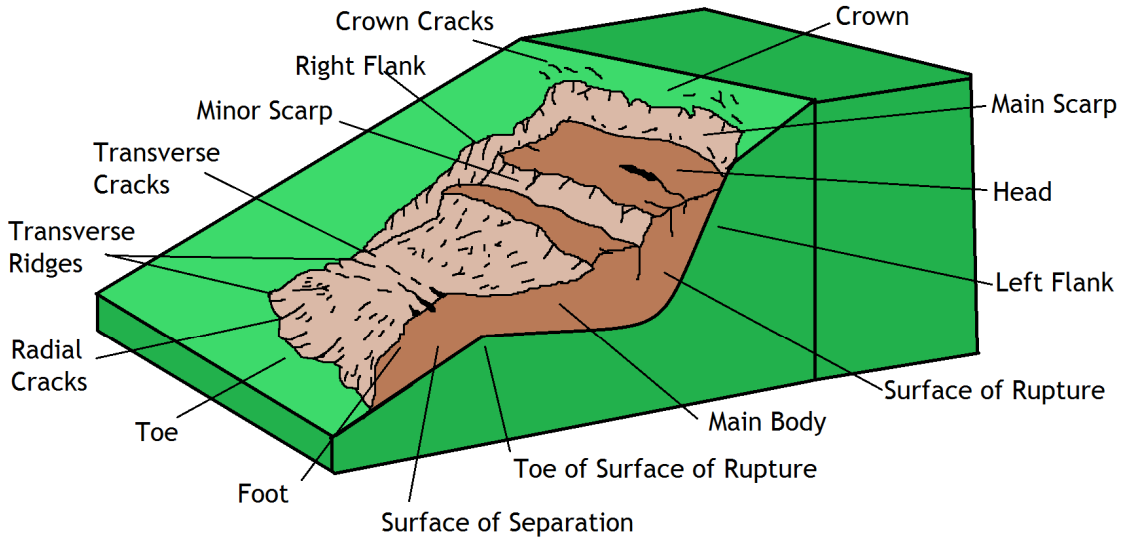

Figure 1. An idealized illustration of a landslide that has evolved to a slump-earth flow. The image also contains the main parts of the landslide with labels (image based on Varnes classification 1978).

The Unmanned Aerial Vehicles (UAVs), or the Remotely Piloted Aircraft Systems (RPAS), or as they are most well-known "drones", are tools that can provide spatial resolution datasets on local or wider scale areas [30,31]. The UAV is a component of an unmanned aircraft/aerial system (UAS), which includes the tool, the pilot and the communication system [32]. During the last decade, the combination of: (a) the rapid development of low cost UAV with improved battery life and (b) the reduction in the dimensions and costs of the optical sensors for civil use have caused a revolution in the photogrammetry surveys and the geohazards investigation [33,34].

UAV-based photogrammetry is able to produce results of high accuracy because of the Structure-from-Motion (SfM) and Scale-Invariant Feature transform (SIFT) algorithms [35]. The SfM is a user-friendly and low-cost alternative to traditional ground-based techniques [36]. The SIFT algorithm and its variants provide invariance to image translation, rotation, and scaling transformations and good robustness to light changes, noise, and affine transformation [37,38]. There are many high performance examples of landslide mapping in two or three dimensional (2D, 3D) model reconstructions and dimension estimations [39–42]. Furthermore, artificial neural networks (ANN), logistic regression, topographic indices and volume empirical equation have been proposed for landslide mapping [43,44]. In relevant studies, CloudCompare software was used (EDF-R&D, TelecomParisTech, 2013) to examine and compare two point clouds (before and after the event) and estimate the volume of the removed material based on change detection algorithms [45].

In this study a quadcopter, the DJI Mavic 2 Pro (DJI, Shenzhen, Guangdong, China) was used to acquire images of a mass movement event in North Greece. The research was conducted in a landslide that happened on 12th June 2019 (Figure 2). The UAV flight followed the rules of the first Greek Drone Regulation of 2017. This Regulation defines the UAVs and categorizes them based on their weight, while it also introduces the guidelines on the flight plan permission registration (if >50 m), flight distance restrictions, a database of drone registrations, a piloting certificate and professional license, safety rules, privacy and data protection, civil liability and environmental protection issues among others [46–48]. The commercially available software Pix4Dmapper Pro (Pix4D S.A., Prilly, Switzerland) was utilized to import the airborne acquired images, develop the orthomosaic of the study area and the Digital Surface Model (DSM). The ArcGIS software (Esri, Redlands, California, USA) was utilized to map the landslide and perform morphometric analysis and measurements. Presented in the following sections are the results of this methodology utilized in a study area in North Greece. The accuracy of this method can help implement targeted nature-based solutions.

(**a**) (**b**)

Figure 2. (**a**) The study area before (2010) and (**b**) the area after the specific landslide event (2019) depicted in aerial photos (Google Earth Images).

2. Materials and Methods

2.1. The Study Area

The study area, as depicted in Figure 3, is near Nea Zichni; a village located in Serres Prefecture of North Greece (Coordinates: Latitude = 41.021582, Longitude = 23.819888 in the World Geodetic System 84-Universal Transverse Mercator coordinate system Zone 34N

(WGS 84/UTM zone 34N). This area is located at the foothills of the Menoikio Mountain and its elevation is around 200 m. The average annual rainfall is 527 mm based on weather data from 1967–2003 [49]. South of the study area there is a known fault that belongs to the Dafnoudi–Nea Zichni fault segment of the greater Serres Fault Zone. The specific segment is quite rectilinear and strikes Northwest–Southeast [50]. The geomorphology of the area is characterized by steep slopes. The slope has been utilized for the continuous supply of drinking water through a dense network of pipelines [51]. At the same time, the construction of a complex Qanat system during the Ottoman period enabled water supply to the settlement and this system is still active [52]. In contrast, a disadvantage of the steep slope is the existence of many gullies because of the intense soil erosion, especially on red beds and other Neogene (Miocene-Pliocene) and Quaternary sediments [53,54]. According to the geologic map of the area (Prosotsani Sheet of Hellenic Survey of Geology and Mineral Exploration—HSGME), the nearest borehole data (Figure 4) and other studies in the greater area, the geology of the area consists of an upper part known as the terrestrial formation of conglomerates with the lower alternative layers of microcobbles, fine-grained sands, red marls generated in lake paleo-environment [55–57]. The settlement of Nea Zichni was developed on the banks of the drained lake of Achinos and its marshes [58,59]. The lake was drained in 1932 due to a vast engineering workplan that also altered the natural route of Strymonas River and had created the Lithotopos dam (~50 km Eastwest) and consequently the Kerkini Lake/Reservoir [60]. A rainfall event that recorded 29 mm/day by two nearby weather stations (Proti 18 km away and Drama 30 km away) took place on 12th June 2019 and resulted in a landslide and other erosion events that are still expanding, especially during precipitation events. The area, apart from the significant change in size visible landslide (soil slump), is also dominated by subsidence phenomena, debris falling, creep and tension cracks, as depicted in Figure 5a. The specific landslide is categorized as a rotational slide based on the Varnes classification system [61]. Historical worldwide records show that rotational slides are among the most widely distributed failures, which generally occur in slopes with a gradient larger than 50° while many cracks (width range 5–420 mm) are often present before initiation of shear deformation, especially in the crown area [62]. Tension cracks (both transverse and radial) are widely present in the middle and lower part (foot and toe, respectively) of the specific landslide [63]. These forces are also visible near the stream channel where high tree falling is evident as depicted in Figure 5b.

The field measurements and drone flights took place on 11th March 2020. The study area is not listed as a restricted flying zone and there are no restrictions for the flight plan according to the Greek Regulations. The area is located along the stream of Agia Paraskeyi that springs at the slopes of Menoikio Mountain, crosses the village and finally discharges into the Strymonas River [64]. At this point a wastewater treatment plant was constructed in 1999 but it is still not operated due to the landslide and subsidence phenomena. Finally, it is easy to access the area from Nea Zichni due to a road that leads to the cemetery which is only 100 m east of the landslide. There are two videos captured by UAV and showing the specific landslide in June https://www.youtube.com/watch?v=WaAJn24xdYQ (accessed on 24 April 2020) [65] and September 2019 https://www.youtube.com/watch?v=Itvm7MEf9IU (accessed on 24 April 2020) [66].

Figure 3. Location map of the study area within the broad region including wastewater treatment plant, road and cemetery. In addition, photos of the event are attached. The landslide phenomena are delimited by the red parallelogram. The landslide is not visible since it had not occurred as of the date of the acquisition of the image, i.e., January 2018.

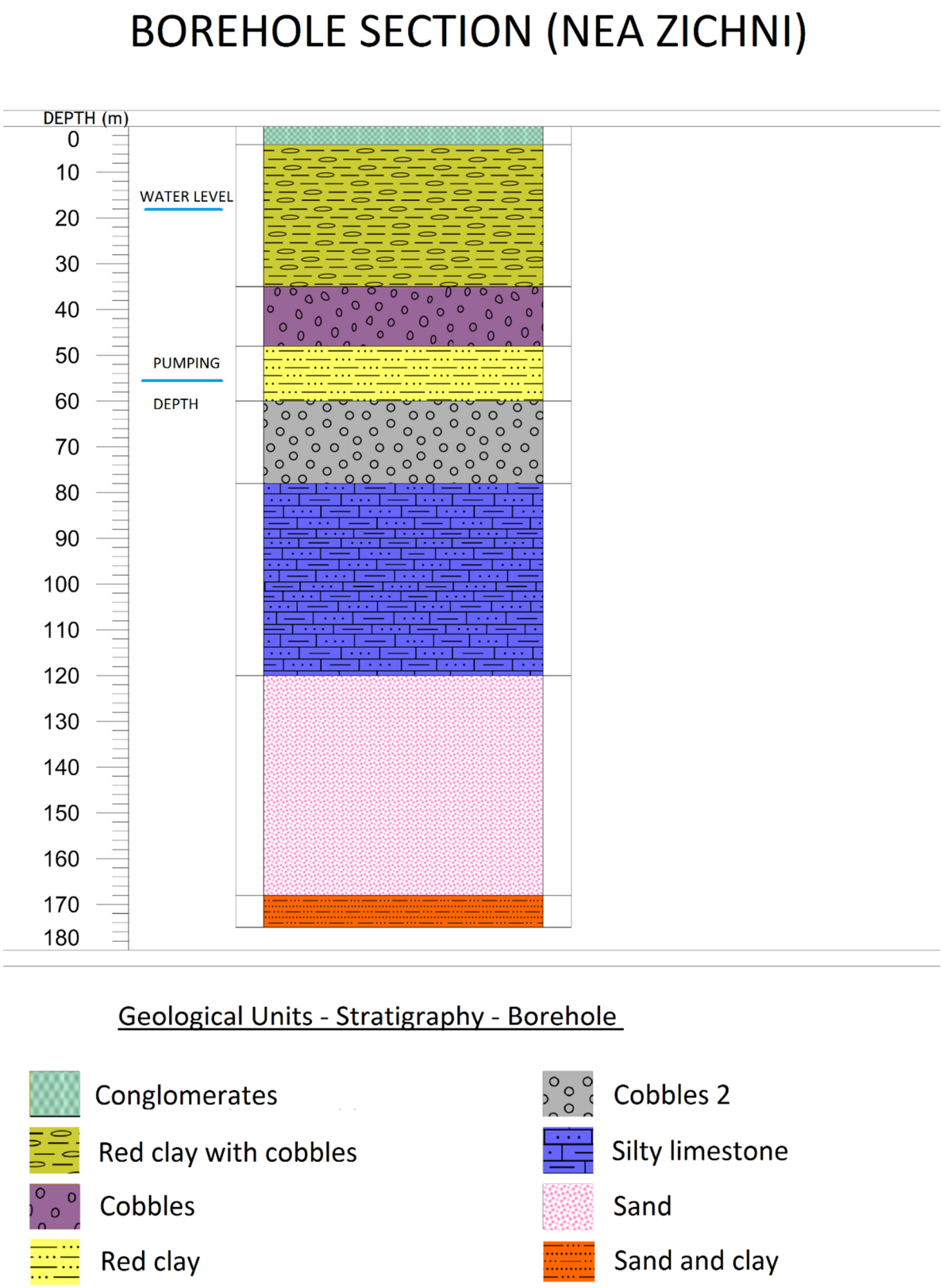

Figure 4. The nearest borehole data near Nea Zichni. The main geological units are depicted based on their depth. In addition, the water level and the water depth of the pump are also depicted.

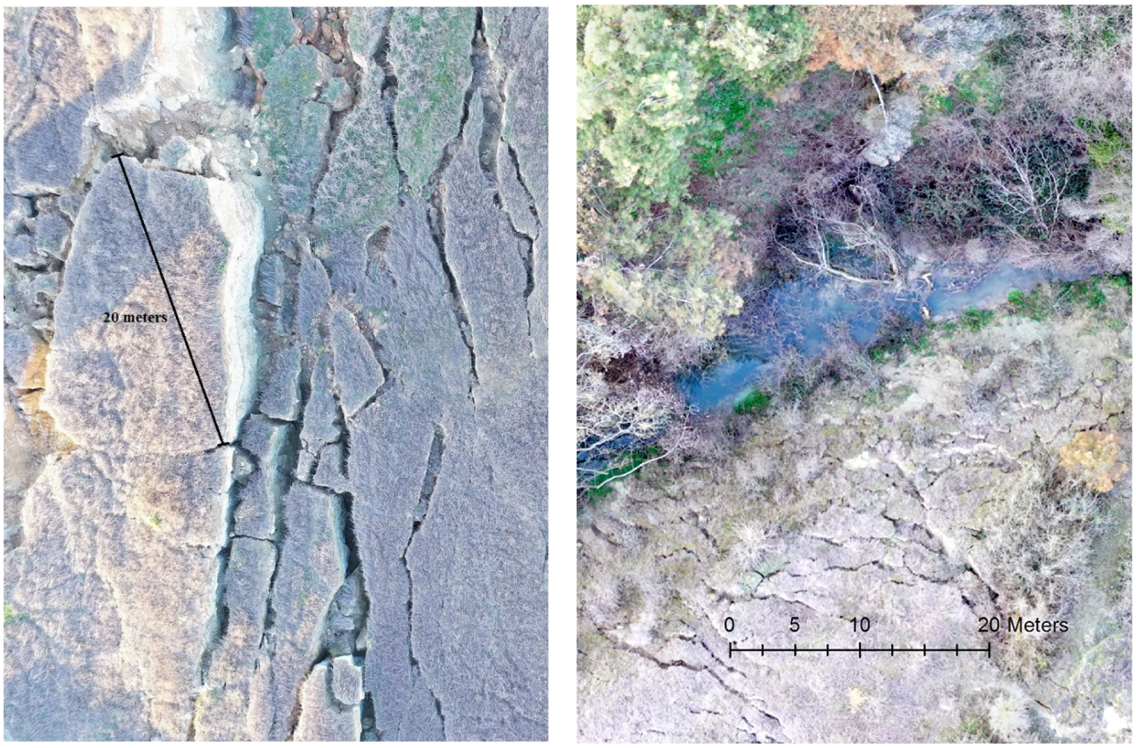

(**a**) (**b**)

Figure 5. (**a**) The cracks of the upper level of the landslide where dominated by topples; (**b**) the nearby stream of Agia Paraskeyi.

2.2. The UAV

The DJI Mavic 2 Pro UAV/RPAS equipped with Hasselblad 20 megapixels digital camera and a complementary metal-oxide-semiconductor (CMOS) sensor was utilized to capture the ortho-images by manually selecting a grid flight plan with frequent intersected images. The specific UAV is a powerful quadcopter capable of flying over large areas as its battery life is 30 min [67]. The DJI Mavic hovered at 50 m and its flight lasted 40′ based on two flights that overlap each other and followed the polygon grid flight plan that covered the study area by capturing 600 images. The ground control points (GCP) included natural points (e.g., trees, rocks), human constructions (e.g., fence, wastewater treatment plant) and artificial marks (e.g., black/white targets in A4 size) were all used in order to georeference and calibrate the produced results. The coordinates were taken by the GPS-GNSS Triumph 1 (Global Positioning System) device (Javad, San Jose, California, USA) and the GPS-GNSS receiver of the UAV. Figure 6 illustrates the topographic land survey and the measuring process of the dimensions by using a tape measure, a laser distance meter and topographic milestones, with the road and the cemetery in the background of the image. The only area that GCPs were not placed was the upper part of the landslide, dominated by topples, because it was considered as a very steep, dangerous area to cross on foot (see Figure 5a). The georeferencing was performed in the Greek Geodetic Reference System coordinate reference system (GGRS87/Greek Grid). The literature offers a wide range of choices for the number and spatial distribution of the GCPs used for photogrammetric applications [68]. In order to create the orthomosaic map and to achieve a good distribution in the widest range of the covered area, 33 GCPs were selected from the total of 71 points that were originally placed and measured (Figure 7). The adjustment points were evenly distributed over the area so that any distortions were uniform. The procedure followed in ArcGIS based on the second polynomial transformation algorithm and the Nearest Neighbor sampling method (Figure 8). These are among the most widely used algorithms introduced to match source and destination ground control points [69]. The mean Root Mean Square Error (RMSE)

was 6.04553 cm while in practice, by using checked coordinates of the GCPs, the accuracy ranged 5 cm–10 cm.

(**a**) (**b**)

Figure 6. (**a**) The topographic survey by using a GPS/GNSS receiver. (**b**) Performing dimension measurements at the crown and scarp of the upper level of the landslide.

(**a**) (**b**)

Figure 7. Examples of the georeferencing methodology in ArcGIS (**a**) of the 10th GCP; (**b**) of the 36th GCP.

2.3. The Software

The Pix4D software uses a modified SfM photogrammetric technique to search and match the points from multiple two-dimensional image sequences resulting from the motion of a camera mounted on UAVs [70]. The software is able to create point clouds, orthomosaics, DSMs as well as an explanatory process report as a pdf file [71]. The Pix4D has many advantages compared to other photogrammetric software as it uses a self-calibration technique and it has a web-based processing service apart from the licensed software [72]. Figure 9 depicts outputs produced by Pix4D based on the used 161 images captured by DJI Mavic 2 Pro. Pix4D was installed in a custom pc that has a 16GB RAM,

AMD Ryzen 3600 processor 3.6 GHz, Nvidia GeForce 1070ti and a SSD disk. According to the statistics provided by the Pix4D report, the average ground sampling distance was 1.44 cm, covered area was 0.178 km^2. The time for initial processing was 24 m 31 s, the time for the DSM generation was 24 m 09 s and the time for orthomosaic generations was 59 m 45 s. The mean camera displacement was 0.010 m, 0.012 m and 0.036 m for longitude, latitude and height, respectively, while georeferencing was included in the WGS 84/UTM zone 34N coordinate system. The initial absolute geolocation variance, produced by Pix4D, resulted to RMSEx = 0.72 m., RMSEy = 1.45 m. and RMSEz = 2.25 m. As mentioned in the previous section, the RMSE was decreased based on the georeferenced process. Finally, the orthomosaic generated in Pix4D was inputted and edited in ArcGIS 10.4 in order to detect and digitize the morphometric parameters of the landslide.

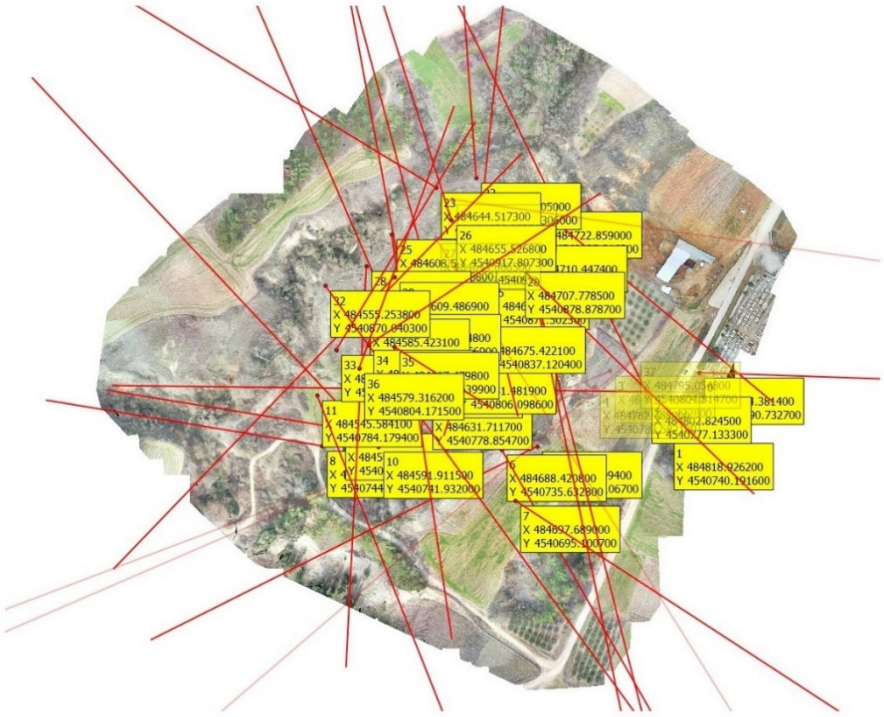

Figure 8. The selections of the proper distributed GCP to georeferenced the orthomosaic and achieve a low RMSE.

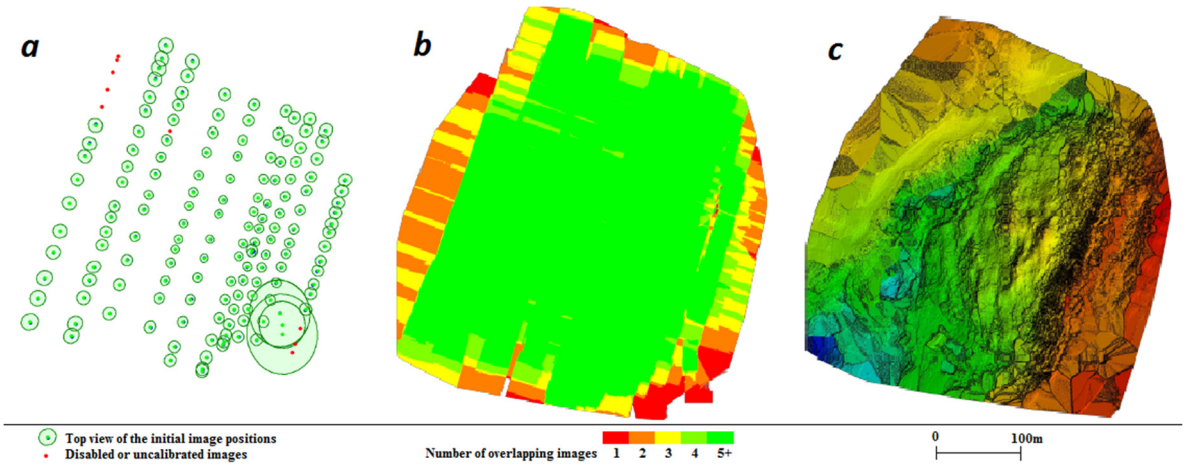

Figure 9. Pix4D processing: (**a**) flight plan–camera positions of the drone survey (green calibrated and included; red disabled or uncalibrated; (**b**) image overlap and (**c**) DSM generated in Pix4D.

3. Results

The Pix4D software generated the orthomosaic based on the georeferenced procedure described above while all of the 600 images were calibrated (100%). The produced output is a hyper-spatial resolution orthomosaic (a) that captured the destruction of the nearby wastewater treatment plant. Figure 10 illustrates the facilities before the event (2016) in Google Maps and the results of the orthomosaic developed by the UAV flight (2020). There is clear evidence that the natural event caused huge destructions in this recent plant construction and specifically at the Northeast part of the two water reservoirs where the walls collapsed (captured inside the red rectangular plan), with the displacement estimated at 2.7 m and the sediments filled the right tank as depicted in the image.

(**a**) (**b**)

Figure 10. The wastewater treatment plant that was constructed in 1999 was captured (**a**) by the satellite image from Google Maps in 2016; (**b**) by the orthomosaic generated in Pix4D in 2020. The destruction of its walls is visible in the NE water tanks (in the red square) that are being filled with sediment.

The orthomosaic was analyzed in ArcGIS 10.4 and the produced result can be seen in Figure 11 that depicts the main landslide (yellow perimeter marked area) and the overall visible affected area (red perimeter marked area), the detected cracks (orange points) on the surface that vary from centimeters to meters. These orange points are representative of the density of the cracks and were detected both in situ and by the hyper-spatial orthomosaic that illustrate even small objects. Based on the detected cracks we also digitized the vectors of these tensile stress cracks or group of cracks (black lines). We further recognized the direction of these tensile stress which are vertical to the digitized tensile stress cracks (black arrows) and hypothesized the most vulnerable cracks for future landslide and subsidence events and topples creation. Specifically, the landslide boundaries were digitized in order to estimate its area. The landslide perimeter was estimated to be 710.2 m while the area was equal to 12,942.6 m^2. Finally, considering the detected cracks we digitized the boundary for the entire affected area (black line perimeter). The entire affected area was at least equal to 46,556.4 m^2 with a perimeter of 1097.6 m. This area could be larger if there are unseen cracks underground or covered by the vegetation (although there are occasions where vegetation helps to identify cracks). Based on the above determined landslide area, the geology of the region (landslide in soils) and an empirical equation [73], the landslide volume was estimated as 18,542.6 m^3.

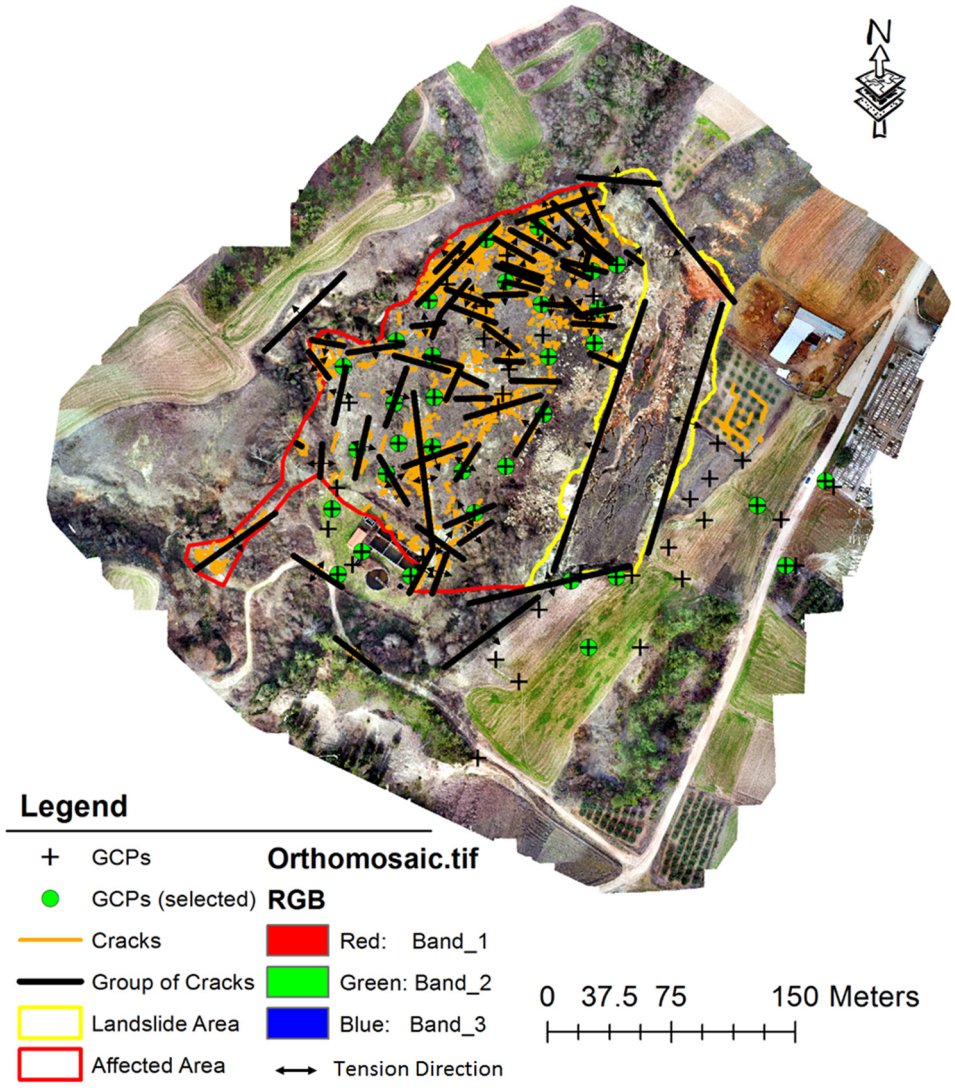

Figure 11. The orthomosaic of the study area depicting the main landslide event (digitized area in yellow) the entire affected area (digitized area in red), the GCPs distributed in the area (black crosses) and the selected ones for georectification (green circles), the detected mapped cracks (orange points), the tensile stress-cracks or group of cracks (black lines) and the direction of the tensile stress (black arrows).

Additionally, we were able to develop the DSM (Figure 12) of the study area which is very useful for topographic, hydrographic and geomorphologic analysis. The DSM was used in order to produce the contour lines of the area (Figure 13). The contour lines were left blank only for the upper part of the landslide, dominated by topples as mentioned before. Furthermore, the DSM can be used as alternative of a digital terrain model (attention must be given in order to avoid high vegetation, e.g., trees) in order to provide the profile of the landslide or cross sections in any direction (Figure 14). The specific profile sections visualize the stream channel found in 30 m and 50 m, respectively, as well as the elevation differences. The graphs also individualize the main parts of the landslide such as the main body of the mass movement, the surface of rupture, the head, the crown and the main scarp. Finally, based on the DSM, another valuable dataset that can be produced is the triangulated irregular network (TIN) which can visualize the 3D surface terrain of the area (Figure 15). The specific dataset can be combined with other 3D models developed in Pix3D (Figure 15) to better reconstruct the natural dimensions of such phenomena. The specific datasets were not further analyzed as we did not intend to study the phenomenon in the 3D without using a total station to calibrate the produced dimensions.

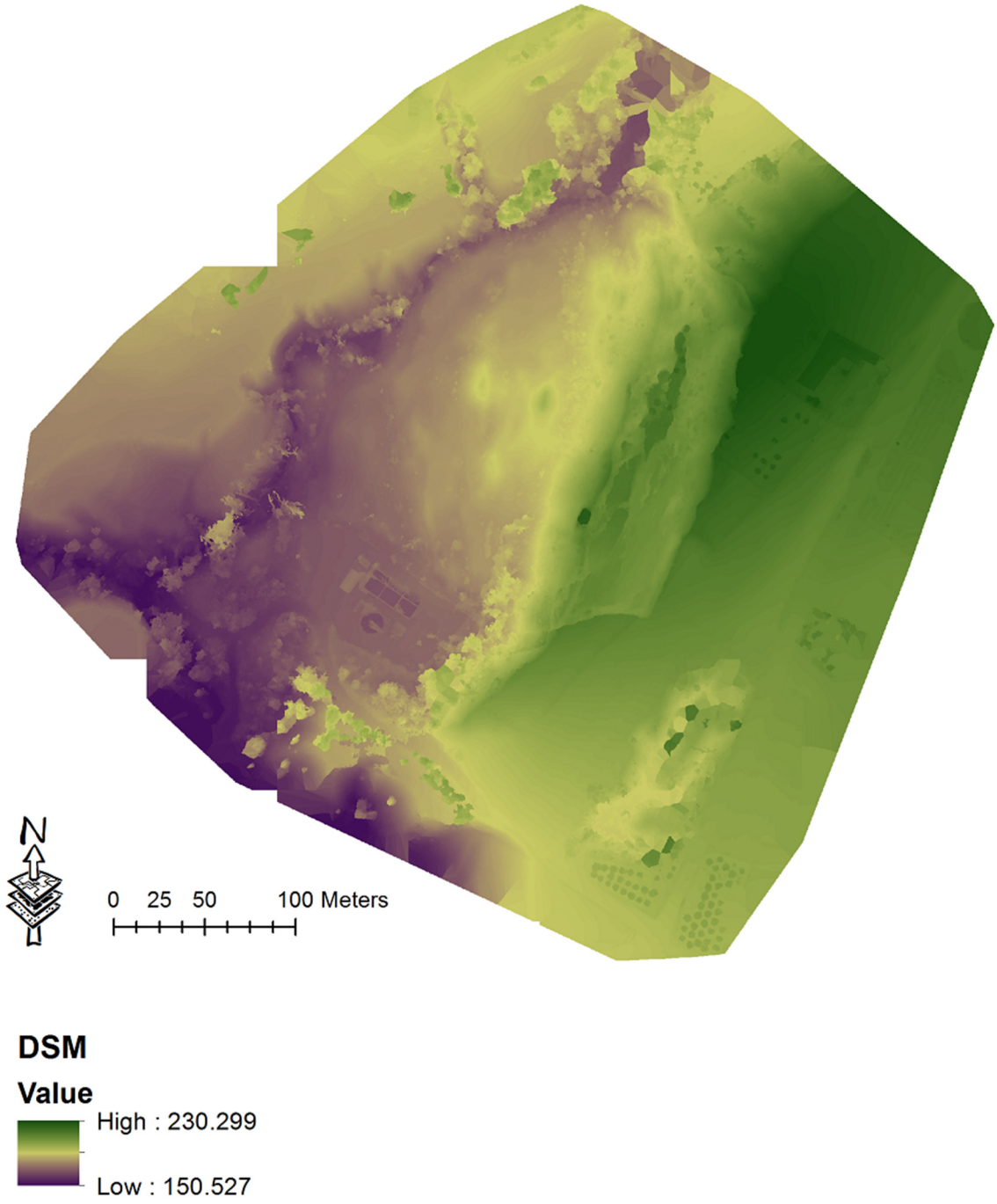

Figure 12. The digital surface model (DSM) of the study area that depicts the entire captured area including the main landslide event, the stream channel and its riparian vegetation, agricultural crops and trees but human-made facilities are also distinguishable.

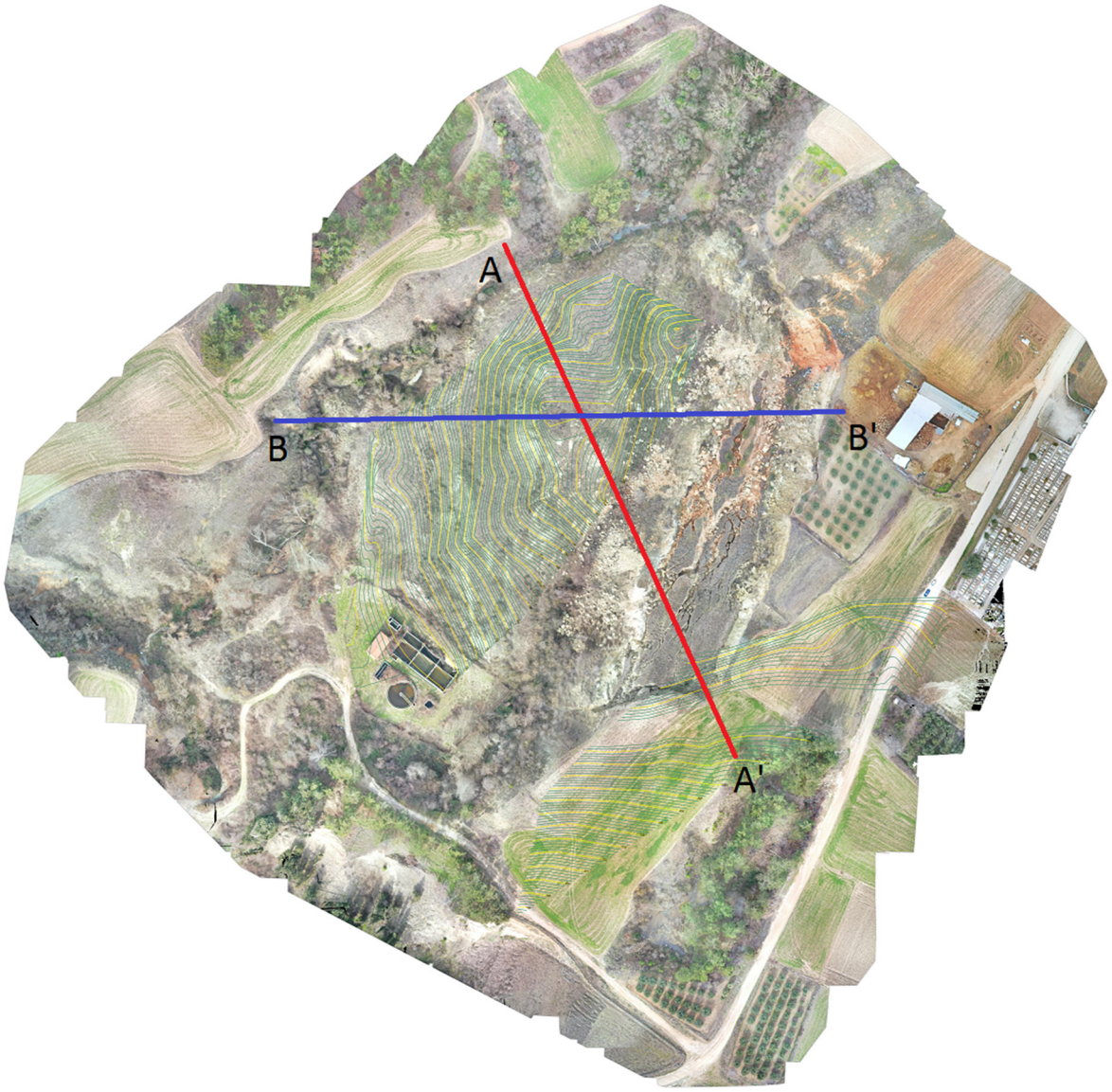

Figure 13. The orthomosaic of the study and the produced contour lines (green parallel curves). Contour lines were not produced in the main landslide area. Two cross sections: the red line (A-A′) and the blue line (B-B′) were selected to visualize the profiles of the study area.

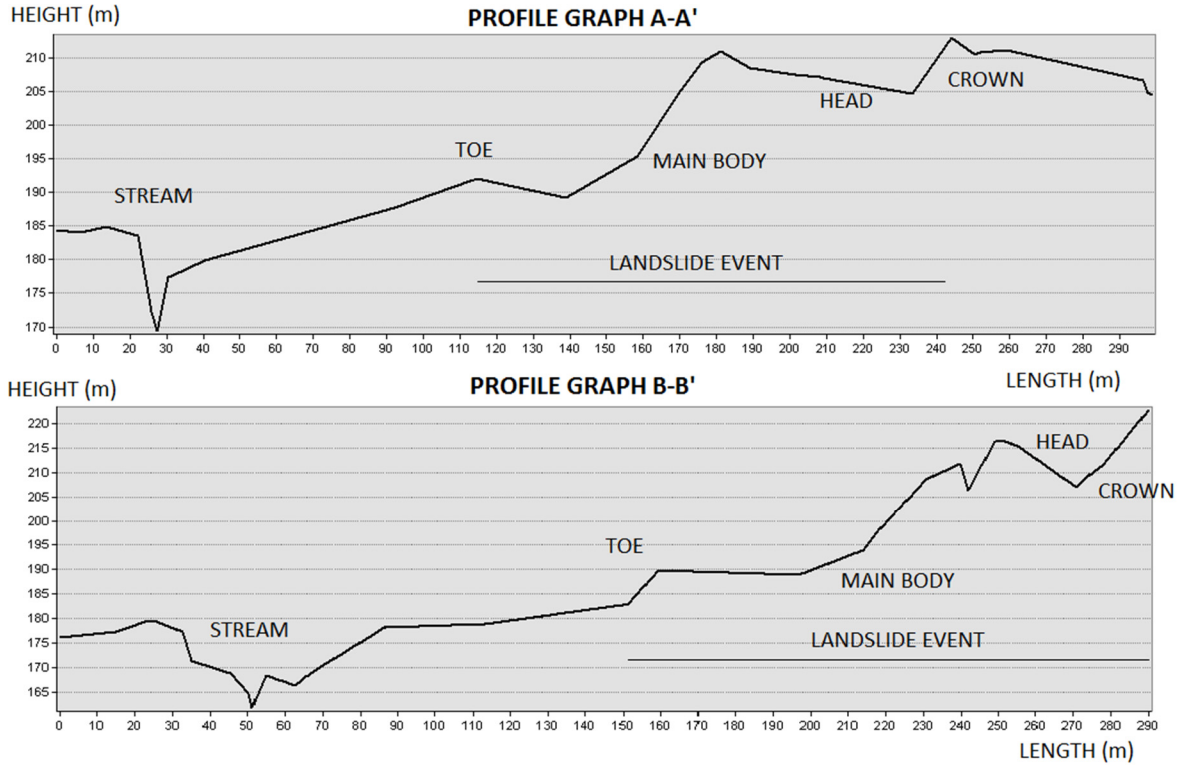

Figure 14. The profiles of the study area: the profile graph A-A′ has a direction from northwest to southeast and the profile graph B-B′ has a direction from west to east.

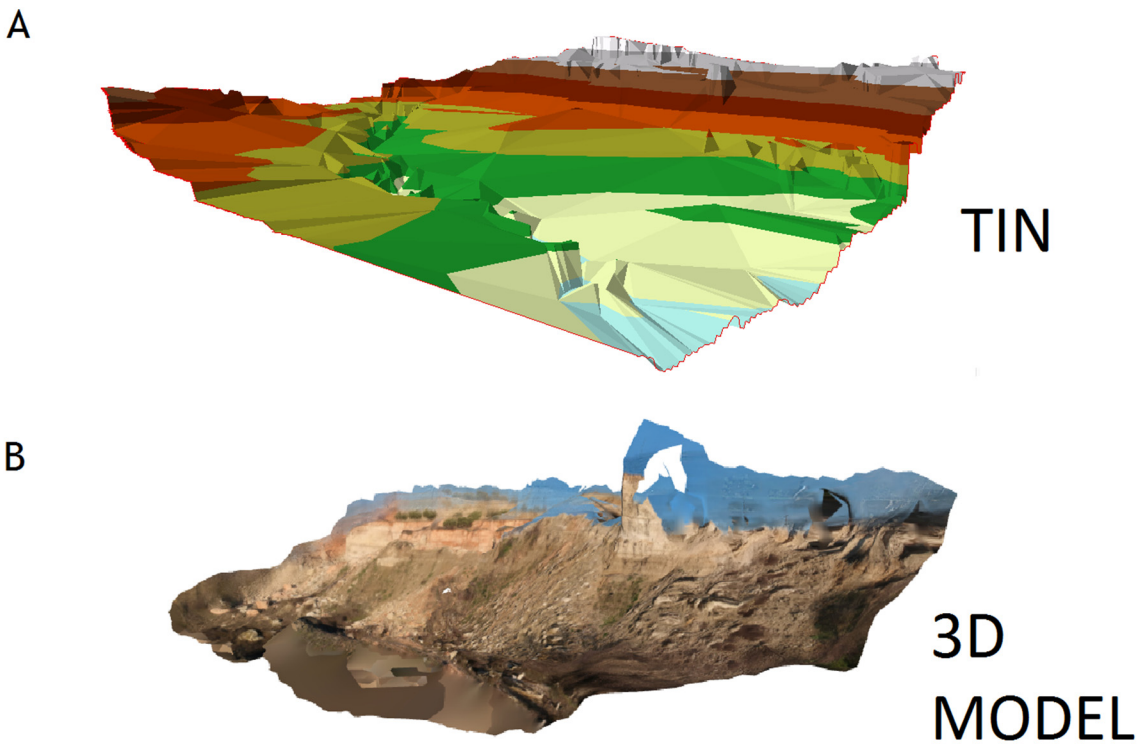

Figure 15. (**A**) The triangulated irregular network (TIN) (top image) developed by the digital surface model (DSM) in ArcGIS and (**B**) the 3D model (bottom image) that was developed in Pix4D. The dimensions are not calibrated to field measurements.

4. Discussion

The aim of this study was to showcase how a UAV (DJI Mavic 2 Pro), a photogrammetric software (Pix4D) and a GIS software (ArcGIS) can be utilized to provide detailed and accurate information on a specific landslide event. A combination of practices including landslide monitoring [74,75] and the mapping of cracks on buildings and asphalt roads [76,77]. Other researchers have also found that UAVs can be used to mitigate risk from natural disasters events such as landslides or subsidence phenomena, or even compared the results among different photogrammetry software [78–80]. To our knowledge, this is innovative work concerning photogrammetric measurements of characteristics and dimensions of the main landslide event and the digitization of the tension cracks of mass movement events based on high-resolution images captured by a low-cost UAV. The digitization of cracks and further spatial and morphometric analysis can be achieved in a short period compared to traditional field mapping and measurements. The overall results are very satisfactory since they can provide valuable information for decision makers, land managers, farmers and other stakeholders. Based on this information the proper Nature-based Solutions (NbS) can be selected to help mitigate the potential negative impacts from the landslide. The methodology described in previous sections provided the morphometric measurements (area of the landslide, elevation difference of the landslide, volume of the affected soil concerning the recent landslide, extended affected area of the landslide and related phenomena, but also the fissures and their tensile stress cracks directions) of a specific landslide and also this information was depicted as maps that are easy to understand and assess. Although this is a preliminary work focused on a small area, it was sufficient to point out some advantages and drawbacks of the technique. Photogrammetry was an accurate method to measure the elevation difference by creating the DSM in our study area and the contour lines in an immediate and rapid approach. This elevation difference was validated based on field measurements and were highly correlated based on the primarily scopes of this study concerning the landslide. It should be noted that the processing time and system requirements are major factors to consider when determining ideal parameters, especially flight altitude or dense overlapping. We found that a computer with 16GB of RAM is a satisfactory selection and the processing was easier and faster to achieve in the specific hardware. Generally, the methodology is user-friendly and easy to implement, which indicates that it could be easily adopted. There are some issues that must be investigated such as the flight regulations and if there are any restricted zones in the area of interest. In addition, the flight plan, the proper hours in a day and the weather conditions necessary in order to capture the best image quality and avoid shadows or inclined views are important factors. Furthermore, the area must be easily accessible in order to carry the necessary equipment while it is mandatory to be conscious and follow safety guidelines as these areas are always dangerous to visit. The above showcase that the method could and should be adopted by public and municipal services responsible for mitigating natural disasters and land management. Finally, the high accuracy of the method could help target areas to mitigate these natural disasters with the use of NbS [81]. NbS is a term defined as "actions to protect, sustainably manage, and restore natural or modified ecosystems that address societal challenges effectively and adaptively, simultaneously providing human well-being and biodiversity benefits" by the International Conservation of Nature (IUCN) [82]. NbS is an umbrella term for various ecosystem-based approaches [83]. Other relevant terms that can be found in the literature, among others, are vegetation engineering, ecosystem engineering, soil bioengeering, ecosystem-based, etc. [84]. For this reason, NbS is usually referred to as green, blue or blue-green solution, as opposed to traditional engineering solutions that represent grey solutions [85]. Bioengineering practices can be considered as the pioneer of NbS for landslide protection since it provides environmentally friendly and cost-effective solutions [86]. Bioengineering solutions for landslides include, among others, the use of living materials. Typical examples are the plant/grass seeding, live transplanting, and other approaches such as wattle fences, brush layers, live fascines or crib walls [87,88]. The most common practice is the use of vegetation

and especially the tree/shrub species, e.g., *Fagus sylvatica* and willow (*Salix* sp.) or mixtures of herbaceous species, e.g., red campion (*Silene dioica Clariv.*) and blue fleabane (*Erigeron acris* L.) which reinforce the soil stability due to their root system elastic strength and anchoring capacity [89,90]. Furthermore, they provide another advantage as they reduce surface runoff and erosion processes due to evapotranspiration. This type of vegetation can be adopted in smooth terrain and even on steep slopes. Especially, woody vegetation (e.g., *Salix* sp.) has a positive slope stability under wetting and drying conditions in shallow landslides [91]. In addition, the use of grass is preferred against surface soil erosion because grasses can develop a good turf and dense root system [92]. The truth is that in deep-seated landslides, soil bioengineering techniques are not enough, so hybrid solutions (conventional engineering solutions which are combined with NbS) are required to maintain or reduce the hazard [93]. Climate change is another factor that densifies such events so the monitoring of such phenomena is highly compulsory. Climate change is expected to lead to more frequent and intense dry/wet periods and will exacerbate the landslide phenomena, especially in the Mediterranean countries [94,95]. This is another reason that highlights the importance of innovative technologies to identify potential landslide areas that will help implement targeted nature-based practices and adaptation actions.

Future research directions could include the utilization of satellite images from previous years in order to compare changes but also performing UAV flights more periodically for the detection of future changes. In addition, the creation of a denser GCP network by using a total station that will cover the entire area, even the area which is dangerous to visit on foot, would be crucial for 3D photogrammetric reconstruction and accurate dimension measurements in these 3D models [96]. Finally, future monitoring could be achieved by using remote sensing or/and ground-based radar interferometry [97,98] and wireless sensor networks for installed ground or underground instruments (e.g., extensometers, inclinometers, piezometers, geophones, ultrasonic signals, etc.) [99].

5. Conclusions

The accuracy of photogrammetry and its application on geohazards has improved within the last years due to the use of digital images, image matching algorithms and the wide application of UAVs. In this study, we used the quadcopter UAV DJI Mavic 2 Pro equipped with a standard digital camera and GPS + GLONASS to collect multi-temporal sets of very high resolution RGB images over a landslide that happened in Northern Greece near the village Nea Zichni. The commercial software Pix4D was selected in order to produce a high-resolution orthomosaic which provided measurements up to cm level. Even small objects could be easily identified. Our results showcase how the combination of UAV-based imagery and SfM algorithms were utilized for 2D and 3D surface reconstruction such as orthomosaic, DSM and TIN. The outputs were further analyzed in ArcGIS software in order to digitize and perform morphometric measurements. The results prove that the tools, software and methodology can be used for the flexible and accurate monitoring of landslides and the mapping of geomorphologic parameters. The specific methodology could be adopted by public and municipal bodies which are responsible for planning and disaster management in order to develop proper management plans and mitigation practices such as nature-based solutions. Finally, additional denser and more frequent research needs to be conducted in order to monitor the evolution of the specific landslide that could be extended and affect a wider area.

Author Contributions: Conceptualization, P.D.K. and G.N.Z.; methodology, P.D.K.; software, P.D.K. and G.T.G.; validation, P.D.K., G.T.G. and G.N.Z.; formal analysis, P.D.K. and O.A.T.; investigation, G.I.P., P.D.K. and G.T.G.; resources, G.I.P., P.D.K. and G.T.G.; data curation, G.I.P., P.D.K. and G.T.G.; writing—original draft preparation, P.D.K. and G.N.Z.; writing—review and editing, G.N.Z. and O.A.T.; visualization, P.D.K., G.I.P. and G.T.G.; supervision, G.N.Z. and O.A.T. All authors have read and agreed to the published version of the manuscript.

Funding: This research received no external funding.

Institutional Review Board Statement: Not applicable.

Informed Consent Statement: Not applicable.

Data Availability Statement: Not applicable.

Conflicts of Interest: The authors declare no conflict of interest.

References

1. Guzzetti, F.; Carrara, A.; Cardinali, M.; Reichenbach, P. Landslide hazard evaluation: A review of current techniques and their application in a multi-scale study, Central Italy. *Geomorphology* **1999**, *31*, 181–216. [CrossRef]
2. Kazeev, A.; Postoev, G. Landslide investigations in Russia and the former USSR. *Nat. Hazards* **2017**, *88*, 81–101. [CrossRef]
3. Bhandari, R.K. Patterns of subsidence in landslides. In Proceedings of the 5th International Symposium on Land Subsidence, The Hague, The Netherlands, 16–20 October 1995; pp. 403–412.
4. Varnes, D.J. Slope movement types and processes. In *Special Report 176: Landslides: Analysis and Control*; Schuster, R.L., Krizek, R.J., Eds.; Transportation and Road Research Board, National Academy of Science: Washington, DC, USA, 1978; pp. 11–33.
5. Hungr, O.; Leroueil, S.; Picarelli, L. The Varnes classification of landslide types, an update. *Landslides* **2014**, *11*, 167–194. [CrossRef]
6. Highland, L.; Bobrowsky, P.T. *The Landslide Handbook: A Guide to Understanding Landslides*; Geological Survey: Reston, PA, USA; p. 129.
7. Rotaru, A.; Oajdea, D.; Răileanu, P. Analysis of the landslide movements. *Int. J. Geol.* **2007**, *1*, 70–79.
8. Loupasakis, C.; Angelitsa, V.; Rozos, D.; Spanou, N. Mining geohazards—Land subsidence caused by the dewatering of opencast coal mines: The case study of the Amyntaio coal mine, Florina, Greece. *Nat. Hazards* **2014**, *70*, 675–691. [CrossRef]
9. Apostolidis, E.; Koukis, G. Engineering-geological conditions of the formations in the Western Thessaly basin. Greece. *Open Geosci.* **2013**, *5*, 407–422. [CrossRef]
10. Psimoulis, P.; Ghilardi, M.; Fouache, E.; Stiros, S. Subsidence and evolution of the Thessaloniki plain, Greece, based on historical leveling and GPS data. *Eng. Geol.* **2007**, *90*, 55–70. [CrossRef]
11. Castañeda, C.; Gutiérrez, F.; Manunta, M.; Galve, J.P. DInSAR measurements of ground deformation by sinkholes, mining subsidence, and landslides, Ebro River, Spain. *Earth Surf. Process. Landf.* **2009**, *34*, 1562–1574. [CrossRef]
12. Du, Z.; Ge, L.; Ng, A.H.M.; Zhu, Q.; Zhang, Q.; Kuang, J.; Dong, Y. Long-term subsidence in Mexico City from 2004 to 2018 revealed by five synthetic aperture radar sensors. *Land Degrad. Dev.* **2019**, *30*, 1785–1801. [CrossRef]
13. Indirli, M.; Knezic, S.; Borg, R.P.; Kaluarachchi, Y.; Ranguelov, B.; Romagnoli, F.; Rochas, C. The ANDROID case study; Venice and its territory: A general overview. *Procedia Econ. Financ.* **2014**, *18*, 837–848. [CrossRef]
14. Shen, S.L.; Xu, Y.S. Numerical evaluation of land subsidence induced by groundwater pumping in Shanghai. *Can. Geotech. J.* **2011**, *48*, 1378–1392. [CrossRef]
15. Mahmoudpour, M.; Khamehchiyan, M.; Nikudel, M.R.; Ghassemi, M.R. Numerical simulation and prediction of regional land subsidence caused by groundwater exploitation in the southwest plain of Tehran, Iran. *Eng. Geol.* **2016**, *201*, 6–28. [CrossRef]
16. Guthrie, R.H.; Mitchell, S.J.; Lanquaye-Opoku, N.; Evans, S.G. Extreme weather and landslide initiation in coastal British Columbia. *Q. J. Eng. Geol. Hydrogeol.* **2010**, *43*, 417–428. [CrossRef]
17. Koukis, G.; Sabatakakis, N.; Ferentinou, M.; Lainas, S.; Alexiadou, X.; Panagopoulos, A. Landslide phenomena related to major fault tectonics: Rift zone of Corinth Gulf, Greece. *Bull. Eng. Geol. Environ.* **2009**, *68*, 215–229. [CrossRef]
18. Bozzano, F.; Cipriani, I.; Mazzanti, P.; Prestininzi, A. Displacement patterns of a landslide affected by human activities: Insights from ground-based InSAR monitoring. *Nat. Hazards* **2011**, *59*, 1377–1396. [CrossRef]
19. Koutalakis, P.; Tzoraki, O.; Zaimes, G.N. Detecting riverbank changes with remote sensing tools. Case study: Aggitis River in Greece. *Analele Universităţii" Dunărea de Jos" din Galaţi. Fascicula II, Matematică, fizică, mecanică teoretică/Ann. Dunarea de Jos Univ. Galati. Fascicle II Math. Phys. Theor. Mech.* **2019**, *42*, 134–142. [CrossRef]
20. Patton, A.I.; Rathburn, S.L.; Capps, D.M. Landslide response to climate change in permafrost regions. *Geomorphology* **2019**, *340*, 116–128. [CrossRef]
21. Tzoraki, O.; Monioudi, I.N.; Velegrakis, A.F.; Moutafis, N.; Pavlogeorgatos, G.; Kitsiou, D. Resilience of touristic island beaches under sea level rise: A methodological framework. *Coast. Manag.* **2018**, *46*, 78–102. [CrossRef]
22. Green, D.R.; Hagon, J.J.; Gómez, C.; Gregory, B.J. Using low-cost UAVs for environmental monitoring, mapping, and modelling: Examples from the coastal zone. In *Coastal Management: Global Challenges and Innovations*; Krishnamurthy, R.R., Jonathan, M.P., Srinivasalu, S., Glaeser, B., Eds.; Elsevier: Amsterdam, The Netherlands, 2019; Volume 20, pp. 465–501.
23. Godone, D.; Allasia, P.; Borrelli, L.; Gullà, G. UAV and Structure from Motion Approach to Monitor the Maierato Landslide Evolution. *Remote Sens.* **2020**, *12*, 1039. [CrossRef]
24. Yaprak, S.; Yildirim, O.; Susam, T.; Inyurt, S.; Oguz, I. The role of Unmanned Aerial Vehicles (UAVs) in monitoring rapidly occurring landslides. *Nat. Hazards Earth Syst. Sci. Discuss.* **2018**, *72*, 1–18.
25. Nikolakopoulos, K.; Kavoura, K.; Depountis, N.; Kyriou, A.; Argyropoulos, N.; Koukouvelas, I.; Sabatakakis, N. Preliminary results from active landslide monitoring using multidisciplinary surveys. *Eur. J. Remote Sens.* **2017**, *50*, 280–299. [CrossRef]
26. Zan, L.; Latini, G.; Piscina, E.; Polloni, G.; Baldelli, P. Landslides early warning monitoring system. In Proceedings of the IEEE International Geoscience and Remote Sensing Symposium, Toronto, ON, Canada, 24–28 June 2002; pp. 188–190.

27. Turner, D.; Lucieer, A.; De Jong, S.M. Time series analysis of landslide dynamics using an unmanned aerial vehicle (UAV). *Remote Sens.* **2015**, *7*, 1736–1757. [CrossRef]
28. Jaboyedoff, M.; Oppikofer, T.; Abellán, A.; Derron, M.H.; Loye, A.; Metzger, R.; Pedrazzini, A. Use of LIDAR in landslide investigations: A review. *Nat. Hazards* **2012**, *61*, 5–28. [CrossRef]
29. Musaev, A.; Wang, D.; Pu, C. LITMUS: A multi-service composition system for landslide detection. *IEEE Trans. Serv. Comput.* **2014**, *8*, 715–726. [CrossRef]
30. Woodget, A.S.; Austrums, R.; Maddock, I.P.; Habit, E. Drones and digital photogrammetry: From classifications to continuums for monitoring river habitat and hydromorphology. *Wiley Interdiscip. Rev. Water* **2017**, *4*, e1222. [CrossRef]
31. Koutalakis, P.; Tzoraki, O.; Zaimes, G. UAVs for hydrologic scopes: Application of a low-cost UAV to estimate surface water velocity by using three different image-based methods. *Drones* **2019**, *3*, 14. [CrossRef]
32. Watts, A.C.; Ambrosia, V.G.; Hinkley, E.A. Unmanned aircraft systems in remote sensing and scientific research: Classification and considerations of use. *Remote Sens.* **2012**, *4*, 1671–1692. [CrossRef]
33. Farina, P.; Rossi, G.; Tanteri, L.; Salvatici, T.; Gigli, G.; Moretti, S.; Casagli, N. The use of multi-copter drones for landslide investigations. In Proceedings of the 3rd North American Symposium on Landslides, Roanoke, VA, USA, 4–8 June 2017; pp. 978–984.
34. Rossi, G.; Tanteri, L.; Tofani, V.; Vannocci, P.; Moretti, S.; Casagli, N. Brief Communication: Use of multicopter drone optical images for landslide mapping and characterization. *Nat. Hazards Earth Syst. Sci. Discuss.* **2017**, 1–14.
35. James, M.R.; Robson, S.; d'Oleire-Oltmanns, S.; Niethammer, U. Optimising UAV topographic surveys processed with structure-from-motion: Ground control quality, quantity and bundle adjustment. *Geomorphology* **2017**, *280*, 51–66. [CrossRef]
36. Manfreda, S.; McCabe, M.F.; Miller, P.E.; Lucas, R.; Pajuelo Madrigal, V.; Mallinis, G.; Dor, E.B.; Helman, D.; Estes, L.; Müllerová, J. On the use of unmanned aerial systems for environmental monitoring. *Remote Sens.* **2018**, *10*, 641. [CrossRef]
37. Rossi, G.; Tanteri, L.; Tofani, V.; Vannocci, P.; Moretti, S.; Casagli, N. Multitemporal UAV surveys for landslide mapping and characterization. *Landslides* **2018**, *15*, 1045–1052. [CrossRef]
38. Zhao, J.; Zhang, X.; Gao, C.; Qiu, X.; Tian, Y.; Zhu, Y.; Cao, W. Rapid mosaicking of unmanned aerial vehicle (UAV) images for crop growth monitoring using the SIFT algorithm. *Remote Sens.* **2019**, *11*, 1226. [CrossRef]
39. Fuhrmann, S.; Langguth, F.; Goesele, M. MVE—A multiview reconstruction environment. In Proceedings of the Eurographics Workshop on Graphics and Cultural Heritage, Darmstadt, Germany, 6–8 October 2014; pp. 11–18.
40. Gupta, S.K.; Shukla, D.P. Application of drone for landslide mapping, dimension estimation and its 3D reconstruction. *J. Indian Soc. Remote Sens.* **2018**, *46*, 903–914. [CrossRef]
41. Lindner, G.; Schraml, K.; Mansberger, R.; Hübl, J. UAV monitoring and documentation of a large landslide. *Appl. Geomat.* **2016**, *8*, 1–11. [CrossRef]
42. Peterman, V. Landslide activity monitoring with the help of unmanned aerial vehicle. *Int. Arch. Photogramm. Remote Sens. Spat. Inf. Sci.* **2015**, *40*, 215. [CrossRef]
43. Lucieer, A.; Jong, S.M.D.; Turner, D. Mapping landslide displacements using Structure from Motion (SfM) and image correlation of multi-temporal UAV photography. *Prog. Phys. Geogr.* **2014**, *38*, 97–116. [CrossRef]
44. Sevgen, E.; Kocaman, S.; Nefeslioglu, H.A.; Gokceoglu, C. A novel performance assessment approach using photogrammetric techniques for landslide susceptibility mapping with logistic regression, ANN and random forest. *Sensors* **2019**, *19*, 3940. [CrossRef] [PubMed]
45. Simonett, D.S. Landslide distribution and earthquakes in the Bavani and Torricelli Mountains, New Guinea. In *Landform Studies from Australia and New Guinea*; Jennings, J.N., Mabbutt, J.A., Eds.; Cambridge University Press: NewYork, NY, USA, 1967; Volume 159, pp. 64–84.
46. Valkaniotis, S.; Papathanassiou, G.; Ganas, A. Mapping an earthquake-induced landslide based on UAV imagery; case study of the 2015 Okeanos landslide, Lefkada, Greece. *Eng. Geol.* **2018**, *245*, 141–152. [CrossRef]
47. Douka, A.K. Drones and environmental protection law in Germany and Greece. In Proceedings of the International Conference on Protection and Restoration of the Environment XIV, Thessaloniki, Greece, 3–6 July 2018; pp. 1076–1082.
48. Tsiamis, N.; Efthymiou, L.; Tsagarakis, K.P. A Comparative Analysis of the Legislation Evolution for Drone Use in OECD Countries. *Drones* **2019**, *3*, 75. [CrossRef]
49. Nigritinos, S. Γεωγραφική κατανομή της βροχόπτωσης στο νομό Σερρών, "Geographical Distribution of Rainfall in the Prefecture of Serres". Bachelor's Thesis, Harokopio University of Athens, Athens, Greece, 2005.
50. Tranos, M.D.; Mountrakis, D.M. The Serres Fault Zone (SFZ): An active fault zone in Eastern Macedonia (Northern Greece). In Proceedings of the 5th International Symposium on Eastern Mediterranean Geology, Thessaloniki, Greece, 14–20 April 2004; Volume 2, pp. 892–895.
51. Prazioutis, I.H. *Ζίχνη-Φυλλίδα, το χρυσάφι των Σερρών, "Zichni-Phyllida, the Gold of Serres"*; Νέα Ζίχνη: [χ.ε.], Greece, 1998.
52. Voudouris, K.S.; Christodoulakos, Y.; Steiakakis, E.; Angelakis, A.N. Hydrogeological Characteristics of Hellenic Aqueducts-Like Qanats. *Water* **2013**, *5*, 1326–1345. [CrossRef]
53. Psilovikos, A.; Vavliakis, E.; Vouvalidis, K.; Papafilippou-Pennou, E. Geomorphological, hydrographical and sedimentological processes at the Serres basin due to quaternary fault tectonics. *Bull. Geol. Soc. Greece BGSG* **2001**, *34*, 451–457. [CrossRef]
54. Beratis, I. Interpretation of the Miocene fossils in the Strymon basin in Northern Greece to determine their habitat. *ASN* **2019**, *6*, 130–144. [CrossRef]

55. Chatzopoulou, M. Μορφοτεκτονικη μελετη του βορειου ρηξιγενους περιθωριου της λεκανης των σερρων, "Morphotectonic Study of North Rift Margin of the Basin of Serres". Master's Thesis, Aristotle University of Thessaloniki, Thessaloniki, Greece, 2017.
56. Andreou, G. Water Supply in Nea Zichni Area. Timeless Approach-Ground Water Quality. Master's Thesis, Aristotle University of Thessaloniki, Thessaloniki, Greece, 2013.
57. Zaimes, G.; Kayiaoglu, K.; Kozanidis, A. Land-use/vegetation cover and soil erosion impacts on soil properties of hilly slopes in Drama Prefecture of Northern Greece. *Kast. Univ. Orman Fak. Derg.* **2017**, *17*, 427–433. [CrossRef]
58. Perrou, T.; Garioud, A.; Parcharidis, I. Use of Sentinel-1 imagery for flood management in a reservoir-regulated river basin. *Front. Earth Sci.* **2018**, *12*, 506–520. [CrossRef]
59. Psilovikos, A.; Margoni, S. An empirical model of sediment deposition processes in Lake Kerkini, Central Macedonia Greece. *Environ. Monit. Assess.* **2010**, *164*, 573–592. [CrossRef] [PubMed]
60. Tsolakidis, I.; Vafiadis, M. Comparison of hydrographic survey and satellite bathymetry in monitoring Kerkini reservoir storage. *Environ. Process.* **2019**, *6*, 1031–1049. [CrossRef]
61. Nemčok, A.; Pašek, J.; Rybář, J. Classification of landslides and other mass movements. *Rock Mech.* **1972**, *4*, 71–78. [CrossRef]
62. Li, Y.; Mo, P. A unified landslide classification system for loess slopes: A critical review. *Geomorphology* **2019**, *340*, 67–83. [CrossRef]
63. Cruden, D.M.; Novograd, S.; Pilot, G.A.; Krauter, E.; Bhandari, R.K.; Cotecchia, V.; Nakamura, H.; Okagbue, C.O.; Zhang, Z.; Ter-Stepanian, G.I. Suggested nomenclature for landslides. *Bull. Int. Assoc. Eng. Geol.* **1990**, *41*, 13–16.
64. Koutalakis, P.; Zaimes, G.N.; Ioannou, K.; Iakovoglou, V. Application of the SWAT model on torrents of the Menoikio, Greece. *Fresenius Environ. Bull.* **2017**, *26*, 1210–1215.
65. Ground Collapsed Next to the Road in an Area of Nea Zichni. Available online: https://www.youtube.com/watch?v=WaAJn24xdYQ (accessed on 24 April 2020).
66. Earth Collapsion by Drone. Available online: https://www.youtube.com/watch?v=Itvm7MEf9IU (accessed on 24 April 2020).
67. Carter, N.; Hashemian, A.; Mckelvey, N. An Optimization of Small Unmanned Aerial System (sUAS) Image Based Scanning Techniques for Mapping Accident Sites. *SAE Int. J. Adv. Curr. Pract. Mobil.* **2019**, *1*, 967–995.
68. Manfreda, S.; Dvorak, P.; Mullerova, J.; Herban, S.; Vuono, P.; Arranz Justel, J.J.; Perks, M. Assessing the accuracy of digital surface models derived from optical imagery acquired with unmanned aerial systems. *Drones* **2019**, *3*, 15. [CrossRef]
69. Tawfeik, H.M.; Hamza, E.; Shawky, A. Determination of suitable requirements for geometric correction of remote sensing satellite images when using ground control points. *Int. Res. J. Eng. Tech.* **2016**, *3*, 54.
70. Pricope, N.G.; Mapes, K.L.; Woodward, K.D.; Olsen, S.F.; Baxley, J.B. Multi-Sensor Assessment of the Effects of Varying Processing Parameters on UAS Product Accuracy and Quality. *Drones* **2019**, *3*, 63. [CrossRef]
71. Covas, J.; Ferreira, V.; Mateus, L. 3D reconstruction with fisheye images strategies to survey complex heritage buildings. In Proceedings of the 2015 Digital Heritage, Granada, Spain, 28 September–2 October 2015; Volume 1, pp. 123–126.
72. Petrie, G. Commercial Operation of Lghtweight UAVs for Aerial Imaging and Mapping: With Particular Reference to the U.K. *GEO Inform.* **2013**, *16*, 28.
73. Larsen, I.J.; Montgomery, D.R.; Korup, O. Landslide erosion controlled by hillslope material. *Nat. Geosci.* **2010**, *3*, 247–251. [CrossRef]
74. Niethammer, U.; James, M.R.; Rothmund, S.; Travelletti, J.; Joswig, M. UAV-based remote sensing of the Super-Sauze landslide: Evaluation and results. *Eng. Geol.* **2012**, *128*, 2–11. [CrossRef]
75. Stumpf, A.; Malet, J.P.; Kerle, N.; Niethammer, U.; Rothmund, S. Image-based mapping of surface fissures for the investigation of landslide dynamics. *Geomorphology* **2013**, *186*, 12–27. [CrossRef]
76. Pan, Y.; Zhang, X.; Cervone, G.; Yang, L. Detection of asphalt pavement potholes and cracks based on the unmanned aerial vehicle multispectral imagery. *IEEE J. Sel. Top. Appl Earth Obs. Remote Sens.* **2018**, *11*, 3701–3712. [CrossRef]
77. Karantanellis, E. Photogrammetry techniques for object-based building crack detection and characterization. In Proceedings of the 16th European Conference in Earthquake Engineering, Thessaloniki, Greece, 18–21 June 2018; pp. 18–21.
78. Yu, M.; Huang, Y.; Zhou, J.; Mao, L. Modeling of landslide topography based on micro-unmanned aerial vehicle photography and structure-from-motion. *Environ. Earth Sci.* **2017**, *76*, 520. [CrossRef]
79. Noferini, L.; Pieraccini, M.; Mecatti, D.; Macaluso, G.; Luzi, G.; Atzeni, C. Long term landslide monitoring by ground-based synthetic aperture radar interferometer. *Int. J. Remote Sens.* **2006**, *27*, 1893–1905. [CrossRef]
80. Intrieri, E.; Gigli, G.; Mugnai, F.; Fanti, R.; Casagli, N. Design and implementation of a landslide early warning system. *Eng. Geol.* **2012**, *147*, 124–136. [CrossRef]
81. Zaimes, G.N.; Tardio, G.; Iakovoglou, V.; Gimenez, M.; Garcia-Rodriguez, J.L.; Sangalli, P. New tools and approaches to promote soil and water bioengineering in the Mediterranean. *Sci. Total Environ.* **2019**, *693*, 133677. [CrossRef] [PubMed]
82. Cohen-Shacham, E.; Walters, G.; Janzen, C.; Maginnis, S. *Nature-Based Solutions to Address Global Societal Challenges*; International Union for Conservation of Nature (IUCN): Gland, Switzerland, 2016; p. 97.
83. Bauduceau, N.; Berry, P.; Cecchi, C.; Elmqvist, T.; Fernandez, M.; Hartig, T.; Krull, H.; Mayerhofer, E.; Sandra, N.; Noring, L.; et al. Towards an EU Research and Innovation Policy Agenda for Nature-Based Solutions and Re-naturing Cities. In *Final Report of the Horizon 2020 Expert Group on 'Nature-Based Solutions and Re-Naturing Cities*; Publications Office of the European Union: Brussels, Belgium, 2015.

84. De Jesús Arce-Mojica, T.; Nehren, U.; Sudmeier-Rieux, K.; Miranda, P.J.; Anhuf, D. Nature-based solutions (NbS) for reducing the risk of shallow landslides: Where do we stand? *Int. J. Disaster Risk Reduct.* **2019**, *41*, 101293. [CrossRef]
85. Solheim, A.; Capobianco, V.; Oen, A.; Kalsnes, B.; Wullf-Knutsen, T.; Olsen, M.; Del Seppia, N.; Arauzo, I.; Balaguer, E.G.; Strout, J.M. Implementing Nature-Based Solutions in Rural Landscapes: Barriers Experienced in the PHUSICOS Project. *Sustainability* **2021**, *13*, 1461. [CrossRef]
86. Kalsnes, B.; Capobianco, V. *Nature-Based Solutions. Landslides Safety Measures*; Klima 2050 Report; SINTEF Academic Press: Trondheim, Norway, 2019; pp. 1–52. ISBN 978-82-536-1638-4.
87. Watkin, L.J.; Ruangpan, L.; Vojinovic, Z.; Weesakul, S.; Torres, A.S. A framework for assessing benefits of implemented nature-based solutions. *Sustainability* **2019**, *11*, 6788. [CrossRef]
88. Kumar, P.; Debele, S.E.; Sahani, J.; Aragão, L.; Barisani, F.; Basu, B.; Bucchignani, E.; Charizopoulos, N.; Di Sabatino, S.; Zieher, T. Towards an operationalisation of nature-based solutions for natural hazards. *Sci. Total Environ.* **2020**, *731*, 138855. [CrossRef]
89. Dhyani, S.; Karki, M.; Gupta, A.K. Opportunities and Advances to Mainstream Nature-Based Solutions in Disaster Risk Management and Climate Strategy. In *Nature-Based Solutions for Resilient Ecosystems and Societies*; Dhyani, S., Gupta, A.K., Karki, M., Eds.; Springer: Singapore, 2020; pp. 1–26.
90. Gonzalez-Ollauri, A.; Mickovski, S.B. Plant-Best: A novel plant selection tool for slope protection. *Ecol. Eng.* **2017**, *106*, 154–173. [CrossRef]
91. Gonzalez-Ollauri, A.; Mickovski, S.B. Hydrological effect of vegetation against rainfall-induced landslides. *J. Hydrol.* **2017**, *549*, 374–387. [CrossRef]
92. Lyons, J.; Thimble, S.W.; Paine, L.K. Grass versus trees: Managing riparian areas to benefit streams of central North America. *JAWRA* **2000**, *36*, 919–930. [CrossRef]
93. Turconi, L.; Faccini, F.; Marchese, A.; Paliaga, G.; Casazza, M.; Vojinovic, Z.; Luino, F. Implementation of Nature-Based Solutions for Hydro-Meteorological Risk Reduction in Small Mediterranean Catchments: The Case of Portofino Natural Regional Park, Italy. *Sustainability* **2020**, *12*, 1240. [CrossRef]
94. Vafeidis, A.T.; Abdulla, A.A.; Bondeau, A.; Brotons, L.; Ludwig, R.; Portman, M.; Reimann, L.; Vousdoukas, M.; Xoplaki, E. Managing future risks and building socio-ecological resilience in the Mediterranean. In *Climate and Environmental Change in the Mediterranean—Current Situation and Risks for the Future. First Mediterranean Assessment Report*; Cramer, W., Guiot, J., Marini, K., Eds.; Union for the Mediterranean, Plan Bleu, UNEP/MAP: Marseille, France, 2020; p. 49, in press.
95. Gariano, S.L.; Guzzetti, F. Landslides in a changing climate. *Earth Sci. Rev.* **2016**, *162*, 227–252. [CrossRef]
96. Zhang, Y.; Tang, H.; Li, C.; Lu, G.; Cai, Y.; Zhang, J.; Tan, F. Design and testing of a flexible inclinometer probe for model tests of landslide deep displacement measurement. *Sensors* **2018**, *18*, 224. [CrossRef]
97. Angeli, M.G.; Pasuto, A.; Silvano, S. A critical review of landslide monitoring experiences. *Eng. Geol.* **2000**, *55*, 133–147. [CrossRef]
98. Zaimes, G.N.; Ioannou, K.; Iakovoglou, V.; Kosmadakis, K.; Koutalakis, P.; Ranis, G.; Emmanouloudis, D.; Schultz, R.C. Improving soil erosion prevention in Greece with new tools. *J. Eng. Sci. Technol.* **2016**, *9*, 66–71. [CrossRef]
99. Savvaidis, P.D. Existing landslide monitoring systems and techniques. In *From Stars to Earth and Culture. In Honor of the Memory of Professor Alexandros*; Dermanis, A., Ed.; School of Rural & Surveying Engineering, The Aristotle University of Thessaloniki: Thessaloniki, Greece, 2003; pp. 242–258.